

Sign-Alternating Thermoelectric Quantum Oscillations and Insulating Landau Levels in Monolayer WTe_2

Yue Tang¹, Tiancheng Song¹, Haosen Guan¹, Yanyu Jia¹, Guo Yu^{1,2}, Zhaoyi Joy Zheng^{1,2}, Ayelet J. Uzan¹, Michael Onyszczyk¹, Ratnadwip Singha³, Xin Gui³, Kenji Watanabe⁴, Takashi Taniguchi⁵, Robert J. Cava³, Leslie M. Schoop³, N. P. Ong¹, Sanfeng Wu^{1*}

¹Department of Physics, Princeton University, Princeton, New Jersey 08544, USA.

²Department of Electrical and Computer Engineering, Princeton University, Princeton, New Jersey 08544, USA.

³Department of Chemistry, Princeton University, Princeton, New Jersey 08544, USA.

⁴Research Center for Electronic and Optical Materials, National Institute for Materials Science, 1-1 Namiki, Tsukuba 305-0044, Japan.

⁵Research Center for Materials Nanoarchitectonics, National Institute for Materials Science, 1-1 Namiki, Tsukuba 305-0044, Japan.

*Correspondence to: sanfengw@princeton.edu

Abstract

The detection of Landau-level-like energy structures near the chemical potential of an insulator is essential to the search for a class of correlated electronic matter hosting charge-neutral fermions and Fermi surfaces, a long-proposed concept that remains elusive experimentally. Here we introduce and demonstrate that the magneto-thermoelectric response of a quantum insulator can reveal critical information not available via other approaches. We report large quantum oscillations (QOs) in the Seebeck response of the hole-doped insulating state of monolayer tungsten ditelluride (WTe_2) in magnetic fields. The QOs remarkably undergo sign-changes as the field is swept, mimicking those in metals with Landau quantization. The sign-change in the thermoelectric response directly implies the presence of a field-induced Landau-level-like structure at the chemical potential of the insulator. Our results reinforce WTe_2 as a platform for investigating insulating Landau levels and mobile neutral fermions in two-dimensional insulators.

Main

While few-layer and bulk $T_d\text{-WTe}_2$ is a compensated semimetal(1), its monolayer form is an insulator with both strong spin-orbit coupling and large exciton binding. Near charge neutrality, the monolayer exhibits the quantum spin Hall effect and is characterized as a topological excitonic insulator (EI)(2–6) (Fig. 1A). When doped with electrons, WTe_2 undergoes a superconducting transition(7, 8) at a critical carrier density $n_c \sim 10^{12} \text{ cm}^{-2}$, with unusual features (9) that lie beyond conventional Landau-Ginzburg description. In sharp contrast, the monolayer, when doped with holes, exhibits a host of unusual properties suggestive of strong correlations at low temperatures (1). In typical samples the system remains insulating up to hole densities of $\sim 10^{13} \text{ cm}^{-2}$ (3–6, 10) (Fig. 1B). Chemical potential measurements reveal a sharp peak in the density of state (DOS) located at the valence band edge(6). This nearly flat dispersion at the valence band edge is accompanied by the formation of the excitonic insulator gap (Fig. 1A). Although localization effects are important in 2D systems, they cannot by themselves account for the observations. The unconventional nature of the hole carriers is also evident in recent experiments on twisted bilayer WTe_2 , in which a 2D anisotropic Luttinger liquid phase was

observed on the hole side and near charge-neutrality, but not on the electron side(11, 12). The nature and properties of hole carriers in 2D WTe₂ are poorly understood. In this work, we report experimental findings of dramatic thermoelectric QOs in the hole-doped insulator state of monolayer WTe₂.

Devices for Detecting Monolayer Thermoelectricity

To examine the thermopower (Seebeck effect) of monolayer WTe₂, we employ the device geometry illustrated in **Fig. 1C**. A heater, made of a thin, narrow and curved Pd strip, is fabricated next to the monolayer WTe₂, which is encapsulated between two graphite/hexagonal boron nitride (hBN) stacks (details in **fig. S1**). Metal electrodes are fabricated to extract electrical signals generated in the monolayer. The vdW stacks allow us to apply gate voltages to either the top (V_{tg}) or bottom (V_{bg}) graphite layers, as well as a temperature gradient $-\nabla T$ within the monolayer plane using the Pd strip heater. An optical image of a device (D1) is shown in **Fig. 1D**. In addition to the thermopower, we also carried out electrical measurements on the device. **Figure 1E** displays the four-probe conductance (G_{xx}) as a function of gate-induced carrier density n_{g} , at selected T . The residual conductance in the insulator state due to transport in the helical edge mode is rapidly suppressed in strong magnetic fields (B) (**Fig. 1F**). Note that here the measurement involves long ($> 10 \mu\text{m}$) and hence resistive edge channels (see the inset of **Fig. 1F**). The monolayer is insulating with a rapidly suppressed conductivity at low T over the entire hole-doped regime (**Fig. 1E**). By contrast, on the electron-rich side we observe signatures of metal-insulator transition and high conductance. These observations are consistent with previous reports(3–5, 10). A similar device geometry has recently enabled successful measurements of the vortex Nernst effect in the electron-rich superconducting state of the monolayer(9). Here we focus on detecting the Seebeck effect of monolayer WTe₂ on the insulating hole-rich side.

Sign-Change of Thermoelectric Quantum Oscillations

For non-interacting fermions, the thermoelectric response function $\alpha = J/|\nabla T|$ (J is the charge current density) is given by $\alpha = 2e \int dE \left(-\frac{\partial f_0}{\partial E} \right) \frac{(E-\mu)}{k_B T} \mathcal{N}(E) v^2 \tau$, where k_B is Boltzmann's constant, e is the elemental charge, f_0 the Fermi-Dirac distribution, μ the chemical potential, $\mathcal{N}(E)$ the DOS, v the group velocity and τ the transport lifetime (the thermopower is $S = \alpha/\sigma$) (13, 14). From the kernel in the equation, we see that α is negative (particle-like) if the derivative $(\partial \mathcal{N} / \partial E)_{\mu} > 0$, and positive (hole-like) if $(\partial \mathcal{N} / \partial E)_{\mu} < 0$. In a magnetic field B , $\mathcal{N}(E, B)$ is the sum of the DOS of individual Landau levels (LLs), approximated by a Lorentzian centered at $E_n = n \hbar \omega_c$ (ω_c is the cyclotron frequency, \hbar is the plank constant and n is an integer index). We infer that, as B is varied, the longitudinal thermoelectric response function $\alpha_{xx}(B)$ changes sign each time E_n crosses μ (**Fig. 2A**). As discussed below, the periodic changes in sign provide a crucial test of the intrinsic nature of the LLs. Such sign changes due to Landau quantization have been observed in semimetals including graphene (15, 16) and few-layer WTe₂ (17).

We investigate the magneto-response of monolayer WTe₂. **Figure 2B** plots the resistance R_{xx} of the monolayer (device D1) at the gate voltages ($V_{\text{tg}} = -3.9 \text{ V}$; $V_{\text{bg}} = -4.5 \text{ V}$). As T decreases, R_{xx} diverges as characteristic of an insulator, reaching $\sim 700 \text{ K}\Omega$ at 2 K. **Figure 2C** plots the magnetoresistance curves which display Shubnikov–de Haas (sdH)-like oscillations. This is surprising as the sample is far from being metallic. The observed QOs in resistance is consistent with the previous report (10).

Our key finding is the QOs in the thermopower in the insulating state. A weak temperature gradient $-\nabla T$ is established in the monolayer by the heater. In the I_s configuration (**Fig. 2D**), the gradient $-\nabla T$ drives a thermoelectric current I_s that flows between the pair of electrodes shorted together (all other contacts are floated). With increasing B , I_s develops QOs, consistent with the oscillations in R_{xx} . Importantly, I_s changes sign whenever R_{xx} displays a local peak. Likewise, oscillations are also observed in the V_s configuration (**Fig. 2E**), in which the selected electrodes are now left open. The voltage difference V_s across them oscillates *v.s.* B , as in the trace of I_s . The oscillations are periodic in $1/B$ and a fast Fourier transformation (FFT) yields the same period of ~ 55.8 T for all three curves (**Fig. 2F**). In large B , the curve of V_s reveals additional sign-changes that coincide with weak maxima seen between the main peaks in R_{xx} . Compared with I_s , V_s seems more sensitive to these features which may arise from, e.g., spin splitting.

The existence of QOs in an insulating material is anomalous. Clearly, we should exclude artefactual mechanisms that could mimic the QOs. The most serious of these assumes that LLs do not exist in the monolayer. For instance, the carrier density n acquires a small oscillatory component δn due to field modulations of e.g., gate capacitance or activated carriers. An oscillating δn may produce changes in R_{xx} . To exclude such mechanisms, it suffices to note that, in such proposals, the thermoelectric current I_s can never change sign since $\delta n < n$ (the same argument applies to V_s). This clearly conflicts with our observations. The present results exclude all mechanisms based on artefactual modulations of the itinerant carrier density of monolayer WTe_2 .

We note that the amplitude of V_s in the high B regime is on the order of $\sim \mu\text{V}$ whereas I_s is $\sim \text{pA}$. Hence the value of V_s/I_s matches the resistance of monolayer WTe_2 qualitatively, a proof that the thermoelectricity is indeed generated in the WTe_2 layer. At low fields ($B < 2$ T), V_s typically vanishes in our devices while I_s might be of a finite value. While we don't fully understand the low- B behavior, we suspect that the presence of edge mode, as well as disorders and localization effects, may play a role in this regime. It is worth mentioning that in graphene the low field thermoelectricity data is less understood as well(**15, 16**). In WTe_2 (**Fig. 2D**), above the onset field $B_{\text{onset}} \sim 3$ T, QOs develop, suggesting a quantum mobility of quasiparticles $\mu \sim 1/B_{\text{onset}} \sim 3300 \text{ cm}^2/(\text{Vs})$. In the standard analysis for SdH oscillations, the period of QOs (~ 55.8 T) indicates a nominal carrier density $n \sim 2.7 \times 10^{12} \text{ cm}^{-2}$ (assuming spin degeneracy). Consequently, we expect from the QO data a conductivity $\sigma = ne\mu \sim 1400 \mu\text{S}$, and hence a good metallicity in the sample. In striking contrast, the resistance (**Figs. 2B & C**) yields a strongly insulating state with a conductivity that is ~ 3 orders of magnitude lower. This is the essential dilemma in the Landau quantization problem of monolayer WTe_2 .

Gate Dependence

The sign-changes in the thermoelectric QOs are observed over a wide hole doping regime. **Fig. 3A** plot R_{xx} *v.s.* V_{tg} while fixing V_{bg} , taken at various T , again demonstrating the insulating behavior in resistance. On the wide hole-rich side, the thermoelectric signals (V_s , as shown in **Fig. 3B**) display QOs with a frequency that is tunable by V_{tg} . The oscillation frequency is however independent of V_{bg} even though V_{bg} does change the overall doping of the sample as indicated in the resistance data (**Figs. 3C & D**). The single-gate dependence of the QO frequency is consistent with previous transport results in the same hole-doped regime(**10, 18**). Note that on the electron side, three QO branches were observed previously in resistance (Extended Data Fig. 4 in ref (**10**)). While here on the hole side the V_{tg} -dependent QO branch is dominant, we can't rule out the possibility that there might

be other branches not seen in the measurements. More discussions on the gate dependence of the QOs will be included in the next section.

The key observation of alternating sign changes induced by B in the V_s , like that seen in **Fig. 2**, is true over a wide gate range (**Figs. 3E-I**). The sign-changes in the thermoelectric QOs and the gate-dependent behaviors are highly reproducible. In **Figs. 3J-N** and **figs. S2-S4**, we present consistent data obtained in another device (D2). **Fig. 4** presents the T dependent of V_s and the QOs. Upon warming up the device to ~ 5 K, the QOs are suppressed altogether along with the vanishing of V_s .

Discussion on Interpretations

QOs in insulators, with a periodicity in $1/B$, have been reported in several systems, including Kondo insulators(19–22), WTe₂ monolayers(10), and α -RuCl₃(23). A comprehensive understanding of the oscillations in these cases is still lacking and the interpretations are widely open including both intrinsic and extrinsic origins(18, 21, 24–39). The mechanisms are likely different in different materials. To firmly establish an intrinsic mechanism of QOs in insulators, it is necessary to detect the same physics in one material using distinct approaches and rule out alternative explanations. In the case of WTe₂ monolayers, proposed mechanisms include (i) magnetic-field induced gap modulations in the excitonic insulator state(31, 32), (ii) modulations of the carrier density due to QOs in the nearby graphite gate(18) and (iii) the presence of mobile charge-neutral fermions in the insulator(10). Scenario (i) is a proposal at charge neutrality where the excitonic insulator forms(31, 32), hence not applicable to the wide hole-doped regime, which is the focus of this work.

Scenario (ii), which attributes the oscillations to the graphite gate, was discussed in the initial report of WTe₂ QOs (10) and subsequently also proposed in ref(18). In the proposal(18), the carrier density of WTe₂ undergoes tiny changes due to small modulations of the gate capacitance in response to QOs in the graphite layer. The resistance of the insulating WTe₂ layer is regarded as a detector of the graphite QOs. The issues raised by this interpretation have been discussed(40, 41). For instance, the fact that the QO frequency depends on one gate voltage but not the other was argued as key evidence supporting this scenario(18). However, this argument relies on an unjustified assumption that the atomically thin WTe₂ insulator screens electric fields perfectly as in the case of an excellent metal (40, 41). The same fact could therefore be argued as evidence against the scenario. The single-gate dependence of the QO frequency is indeed a puzzling observation and a comprehensive understanding is still needed. However, we note that in systems with multi-band carriers, especially with excitons, the expectation for the gate-dependence in a dual-gated device is no longer simple and universal. Recently, single gate dependent behaviors of a 2D device have been observed even in graphene systems(42–44). More importantly, as we already discussed, the periodic sign changes in the thermoelectric QOs are in direct conflict with the proposal of ref (18) (δn induced by the capacitance cannot alter the sign of the thermoelectric signals, which is observed over a wide hole doping range). As explained, the sign-change of I_s or V_s implies a qualitative change of the carriers from being “electron-like” to “hole-like” induced by B , regardless of n_g . The sign change effectively precludes such artefacts arising from the graphite gate.

The striking constraints inferred from the new observations invite us to examine the neutral-fermion scenario (iii). The sign-changing thermoelectric QOs imply that $\mathcal{N}(\mu)$ is strongly modulated in B , much like conventional LLs. The essential dilemma - the violation of $\sigma = ne\mu$ - can be reconciled if we

assume the high-mobility quasiparticles are charge neutral, but still responsible for the observed QOs. One scenario is that holes in monolayer WTe_2 undergo spin-charge separation at low T , i.e., holes split into charged holons and charge-neutral spinons. The experimental observations of a high DOS at valence band edge of the monolayer(6) and the appearance of a 2D anisotropic Luttinger liquid phase on the hole side of twisted bilayers(11, 12) indicates that spin-charge separation in WTe_2 could be possible. If these assumptions are valid, then the localization of holons can cause the insulating behavior in the hole-doped regime of the monolayer whereas the mobile spinons form neutral Fermi surfaces. In B , the spinon band undergoes Landau quantization, similar to that proposed in the context of quantum spin liquid(45) and mixed-valence insulators(37, 46). Both electrical and thermoelectric transport can detect the QOs induced by spinon Landau quantization according to the Ioffe–Larkin rule(47, 48). The spinon LLs are responsible for the sign-changes of the thermoelectric signals. Our results invite an in-depth analysis of hole carriers in WTe_2 and thermoelectric transport in spin-charge separated 2D systems.

Summary and Outlook

The observation of QOs in both electrical and thermoelectric transport places WTe_2 at a unique position for investigating unconventional Landau quantization and possible neutral fermions in insulators. The detection of the same underlying physics using distinct experimental approaches is key to fully addressing the paradox of QOs in insulators. Beyond transport, recent developments of far-infrared magneto-optical spectroscopy for 2D materials at millikelvin temperatures(49) may provide further insights. Beyond WTe_2 , the results and approaches developed along this endeavor will be useful in general for discovering next-generation quantum phenomena in correlated 2D crystals and vdW stacks, especially insulators with fractionalized charge-neutral excitations.

References

1. M. N. Ali, J. Xiong, S. Flynn, J. Tao, Q. D. Gibson, L. M. Schoop, T. Liang, N. Haldolaarachchige, M. Hirschberger, N. P. Ong, R. J. Cava, Large, non-saturating magnetoresistance in WTe_2 . *Nature* **514**, 205–208 (2014).
2. X. Qian, J. Liu, L. Fu, J. Li, Quantum spin Hall effect in two-dimensional transition metal dichalcogenides. *Science* **346**, 1344–1347 (2014).
3. Z. Fei, T. Palomaki, S. Wu, W. Zhao, X. Cai, B. Sun, P. Nguyen, J. Finney, X. Xu, D. H. Cobden, Edge conduction in monolayer WTe_2 . *Nat Phys* **13**, 677–682 (2017).
4. S. Wu, V. Fatemi, Q. D. Gibson, K. Watanabe, T. Taniguchi, R. J. Cava, P. Jarillo-Herrero, Observation of the quantum spin Hall effect up to 100 kelvin in a monolayer crystal. *Science* **359**, 76–79 (2018).
5. Y. Jia, P. Wang, C.-L. Chiu, Z. Song, G. Yu, B. Jäck, S. Lei, S. Klemen, F. A. Cevallos, M. Onyszczak, N. Fishchenko, X. Liu, G. Farahi, F. Xie, Y. Xu, K. Watanabe, T. Taniguchi, B. A. Bernevig, R. J. Cava, L. M. Schoop, A. Yazdani, S. Wu, Evidence for a monolayer excitonic insulator. *Nat Phys* **18**, 87–93 (2022).
6. B. Sun, W. Zhao, T. Palomaki, Z. Fei, E. Runburg, P. Malinowski, X. Huang, J. Cenker, Y.-T. Cui, J.-H. Chu, X. Xu, S. S. Ataie, D. Varsano, M. Palummo, E. Molinari, M. Rontani, D. H. Cobden, Evidence for equilibrium exciton condensation in monolayer WTe_2 . *Nat Phys* **18**, 94–99 (2022).
7. V. Fatemi, S. Wu, Y. Cao, L. Bretheau, Q. D. Gibson, K. Watanabe, T. Taniguchi, R. J. Cava, P. Jarillo-Herrero, Electrically tunable low-density superconductivity in a monolayer topological insulator. *Science* **362**, 926–929 (2018).

8. E. Sajadi, T. Palomaki, Z. Fei, W. Zhao, P. Bement, C. Olsen, S. Luescher, X. Xu, J. A. Folk, D. H. Cobden, Gate-induced superconductivity in a monolayer topological insulator. *Science* **362**, 922–925 (2018).
9. T. Song, Y. Jia, G. Yu, Y. Tang, P. Wang, R. Singha, X. Gui, A. J. Uzan-Narovlansky, M. Onyszczak, K. Watanabe, T. Taniguchi, R. J. Cava, L. M. Schoop, N. P. Ong, S. Wu, Unconventional superconducting quantum criticality in monolayer WTe₂. *Nat Phys* **20**, 269–274 (2024).
10. P. Wang, G. Yu, Y. Jia, M. Onyszczak, F. A. Cevallos, S. Lei, S. Klemenz, K. Watanabe, T. Taniguchi, R. J. Cava, L. M. Schoop, S. Wu, Landau quantization and highly mobile fermions in an insulator. *Nature* **589**, 225–229 (2021).
11. P. Wang, G. Yu, Y. H. Kwan, Y. Jia, S. Lei, S. Klemenz, F. A. Cevallos, R. Singha, T. Devakul, K. Watanabe, T. Taniguchi, S. L. Sondhi, R. J. Cava, L. M. Schoop, S. A. Parameswaran, S. Wu, One-dimensional Luttinger liquids in a two-dimensional moiré lattice. *Nature* **605**, 57–62 (2022).
12. G. Yu, P. Wang, A. J. Uzan, Y. Jia, M. Onyszczak, R. Singha, X. Gui, T. Song, Y. Tang, K. Watanabe, T. Taniguchi, R. J. Cava, L. M. Schoop, S. Wu, Evidence for Two Dimensional Anisotropic Luttinger Liquids at Millikelvin Temperatures. *Nat Commun* **14**, 7025 (2023).
13. M. Cutler, N. F. Mott, Observation of Anderson Localization in an Electron Gas. *Physical Review* **181**, 1336–1340 (1969).
14. J. M. Ziman, *Principles of the Theory of Solids* (Cambridge Univ. Press, 2nd Ed., 1979).
15. J. G. Checkelsky, N. P. Ong, Thermopower and Nernst effect in graphene in a magnetic field. *Phys Rev B* **80**, 81413 (2009).
16. Y. M. Zuev, W. Chang, P. Kim, Thermoelectric and Magnetothermoelectric Transport Measurements of Graphene. *Phys Rev Lett* **102**, 96807 (2009).
17. R. Bi, Z. Feng, X. Li, J. Zhao, J. Fan, Y. Shi, D. Yu, X. Wu, Quantum oscillations of thermopower in WTe₂ thin films. *Phys Rev B* **100**, 235405 (2019).
18. J. Zhu, T. Li, A. F. Young, J. Shan, K. F. Mak, Quantum Oscillations in Two-Dimensional Insulators Induced by Graphite Gates. *Phys Rev Lett* **127**, 247702 (2021).
19. B. S. Tan, Y.-T. Hsu, B. Zeng, M. C. Hatnean, N. Harrison, Z. Zhu, M. Hartstein, M. Kiourlappou, A. Srivastava, M. D. Johannes, T. P. Murphy, J.-H. Park, L. Balicas, G. G. Lonzarich, G. Balakrishnan, S. E. Sebastian, Unconventional Fermi surface in an insulating state. *Science* **349**, 287–290 (2015).
20. G. Li, Z. Xiang, F. Yu, T. Asaba, B. Lawson, P. Cai, C. Tinsman, A. Berkley, S. Wolgast, Y. S. Eo, D.-J. Kim, C. Kurdak, J. W. Allen, K. Sun, X. H. Chen, Y. Y. Wang, Z. Fisk, L. Li, Two-dimensional Fermi surfaces in Kondo insulator SmB₆. *Science* **346**, 1208–1212 (2014).
21. L. Li, K. Sun, C. Kurdak, J. W. Allen, Emergent mystery in the Kondo insulator samarium hexaboride. *Nature Reviews Physics* **2**, 463–479 (2020).
22. Z. Xiang, Y. Kasahara, T. Asaba, B. Lawson, C. Tinsman, L. Chen, K. Sugimoto, S. Kawaguchi, Y. Sato, G. Li, S. Yao, Y. L. Chen, F. Iga, J. Singleton, Y. Matsuda, L. Li, Quantum oscillations of electrical resistivity in an insulator. *Science* **362**, 65–69 (2018).
23. P. Czajka, T. Gao, M. Hirschberger, P. Lampen-Kelley, A. Banerjee, J. Yan, D. G. Mandrus, S. E. Nagler, N. P. Ong, Oscillations of the thermal conductivity in the spin-liquid state of α -RuCl₃. *Nat Phys* **17**, 915–919 (2021).
24. J. Knolle, N. R. Cooper, Quantum Oscillations without a Fermi Surface and the Anomalous de Haas–van Alphen Effect. *Phys Rev Lett* **115**, 146401 (2015).
25. J. Knolle, N. R. Cooper, Anomalous de Haas–van Alphen Effect in InAs/GaSb Quantum Wells. *Phys Rev Lett* **118**, 176801 (2017).
26. H. Shen, L. Fu, Quantum Oscillation from In-Gap States and a Non-Hermitian Landau Level Problem. *Phys Rev Lett* **121**, 026403 (2018).
27. P. Ram, B. Kumar, Theory of quantum oscillations of magnetization in Kondo insulators. *Phys Rev B* **96**, 075115 (2017).

28. O. Erten, P.-Y. Chang, P. Coleman, A. M. Tsvelik, Skyrme Insulators: Insulators at the Brink of Superconductivity. *Phys Rev Lett* **119**, 057603 (2017).
29. L. Zhang, X.-Y. Song, F. Wang, Quantum Oscillation in Narrow-Gap Topological Insulators. *Phys Rev Lett* **116**, 046404 (2016).
30. N. R. Cooper, J. Kelsall, Quantum oscillations in an impurity-band Anderson insulator. *SciPost Physics* **15**, 118 (2023).
31. P. A. Lee, Quantum oscillations in the activated conductivity in excitonic insulators: Possible application to monolayer WTe₂. *Phys Rev B* **103**, L041101 (2021).
32. W.-Y. He, P. A. Lee, Quantum oscillation of thermally activated conductivity in a monolayer WTe₂-like excitonic insulator. *Phys Rev B* **104**, L041110 (2021).
33. J. A. N. Bruin, R. R. Claus, Y. Matsumoto, J. Nuss, S. Laha, B. V. Lotsch, N. Kurita, H. Tanaka, H. Takagi, Origin of oscillatory structures in the magnetothermal conductivity of the putative Kitaev magnet α -RuCl₃. *APL Mater* **10** (2022).
34. S. Suetsugu, Y. Ukai, M. Shimomura, M. Kamimura, T. Asaba, Y. Kasahara, N. Kurita, H. Tanaka, T. Shibauchi, J. Nasu, Y. Motome, Y. Matsuda, Evidence for a Phase Transition in the Quantum Spin Liquid State of a Kitaev Candidate α -RuCl₃. *J Physical Soc Japan* **91** (2022).
35. É. Lefrançois, J. Baglo, Q. Barthélemy, S. Kim, Y.-J. Kim, L. Taillefer, Oscillations in the magnetothermal conductivity of α -RuCl₃: Evidence of transition anomalies. *Phys Rev B* **107**, 064408 (2023).
36. Z. Heda, et al, Anisotropy of thermal conductivity oscillations in relation to the Kitaev spin liquid phase. *arXiv:2310.03917* (2023).
37. I. Sodemann, D. Chowdhury, T. Senthil, Quantum oscillations in insulators with neutral Fermi surfaces. *Phys Rev B* **97**, 045152 (2018).
38. S. M. Thomas, X. Ding, F. Ronning, V. Zapf, J. D. Thompson, Z. Fisk, J. Xia, P. F. S. Rosa, Quantum Oscillations in Flux-Grown SmB₆ with Embedded Aluminum. *Phys Rev Lett* **122**, 166401 (2019).
39. H. Pirie, E. Mascot, C. E. Matt, Y. Liu, P. Chen, M. H. Hamidian, S. Saha, X. Wang, J. Paglione, G. Luke, D. Goldhaber-Gordon, C. F. Hirjibehedin, J. C. S. Davis, D. K. Morr, J. E. Hoffman, Visualizing the atomic-scale origin of metallic behavior in Kondo insulators. *Science* **379**, 1214–1218 (2023).
40. P. Wang, S. Wu, Comments on quantum oscillations in two-dimensional insulators induced by graphite gates. *arXiv:2112.07138* (2021).
41. Sanfeng Wu, The Detection of Unconventional Quantum Oscillations in Insulating 2D Materials. *Accepted to 2D Materials*, arXiv 2024.
42. Z. Zheng, Q. Ma, Z. Bi, S. de la Barrera, M.-H. Liu, N. Mao, Y. Zhang, N. Kiper, K. Watanabe, T. Taniguchi, J. Kong, W. A. Tisdale, R. Ashoori, N. Gedik, L. Fu, S.-Y. Xu, P. Jarillo-Herrero, Unconventional ferroelectricity in moiré heterostructures. *Nature* **588**, 71–76 (2020).
43. R. Niu, Z. Li, X. Han, Z. Qu, D. Ding, Z. Wang, Q. Liu, T. Liu, C. Han, K. Watanabe, T. Taniguchi, M. Wu, Q. Ren, X. Wang, J. Hong, J. Mao, Z. Han, K. Liu, Z. Gan, J. Lu, Giant ferroelectric polarization in a bilayer graphene heterostructure. *Nat Commun* **13**, 6241 (2022).
44. Z. Zheng, X. Wang, Z. Zhu, S. Carr, T. Devakul, S. de la Barrera, N. Paul, Z. Huang, A. Gao, Y. Zhang, D. Bérubé, K. N. Evanco, K. Watanabe, T. Taniguchi, L. Fu, Y. Wang, S.-Y. Xu, E. Kaxiras, P. Jarillo-Herrero, Q. Ma, Electronic ratchet effect in a moire system: signatures of excitonic ferroelectricity. (2023).
45. O. I. Motrunich, Orbital magnetic field effects in spin liquid with spinon Fermi sea: Possible application to κ -(ET)₂(Cu)₂(CN)₃. *Phys Rev B* **73**, 155115 (2006).
46. D. Chowdhury, I. Sodemann, T. Senthil, Mixed-valence insulators with neutral Fermi surfaces. *Nat Commun* **9**, 1766 (2018).

47. L. B. Ioffe, A. I. Larkin, Gapless fermions and gauge fields in dielectrics. *Phys Rev B* **39**, 8988–8999 (1989).
48. P. A. Lee, N. Nagaosa, Gauge theory of the normal state of high- T_c superconductors. *Phys Rev B* **46**, 5621–5639 (1992).
49. M. Onyszczak, A. J. Uzan-Narovlansky, Y. Tang, P. Wang, Y. Jia, G. Yu, T. Song, R. Singha, J. F. Khoury, L. M. Schoop, S. Wu, A platform for far-infrared spectroscopy of quantum materials at millikelvin temperatures. *Review of Scientific Instruments* **94** (2023).

Acknowledgments

This work is mainly supported by the NSF through the Materials Research Science and Engineering Center (MRSEC) program of the National Science Foundation (DMR-2011750) through support to S.W., L. M. S. and R.J.C., and a CAREER award (DMR-1942942) to S.W. S.W. also acknowledges support from AFOSR through a Young Investigator Award (FA9550-23-1-0140), ONR through a Young Investigator Award (N00014-21-1-2804), the Gordon and Betty Moore Foundation through Grant GBMF11946 and the Sloan Foundation. L.M.S. acknowledges support from the Gordon and Betty Moore Foundation's EPIQS initiative through Grant GBMF9064 and the David and Lucile Packard Foundation. S.W. and L.M.S. acknowledge support from the Eric and Wendy Schmidt Transformative Technology Fund at Princeton. R. J. C. at Princeton acknowledges support from the Gordon and Betty Moore Foundation through grant GBMF-9066 and the US DOE division of Basic Energy Sciences (DE-FG02-98R45706). T.S. acknowledges support from the Princeton Physics Dicke Fellowship program. A.J.U acknowledges support from the Rothschild Foundation and the Zuckerman Foundation. K.W. and T.T. acknowledge support from the JSPS KAKENHI (Grant Numbers 20H00354 and 23H02052) and World Premier International Research Center Initiative (WPI), MEXT, Japan.

Author contributions

S.W. conceived, designed and supervised the project. Y.T. fabricated the devices and performed measurements, assisted by T.S., H.G., Y.J., G.Y. Z.J.Z., A.J.U., and M.O. R.S. L.M.S., X.G. and R.J.C grew bulk WTe_2 crystals. K.W. and T.T. provided hBN crystals. S.W., N.P.O. and Y. T. analyzed the data, interpreted the results, and wrote the paper with input from all authors.

Competing interests

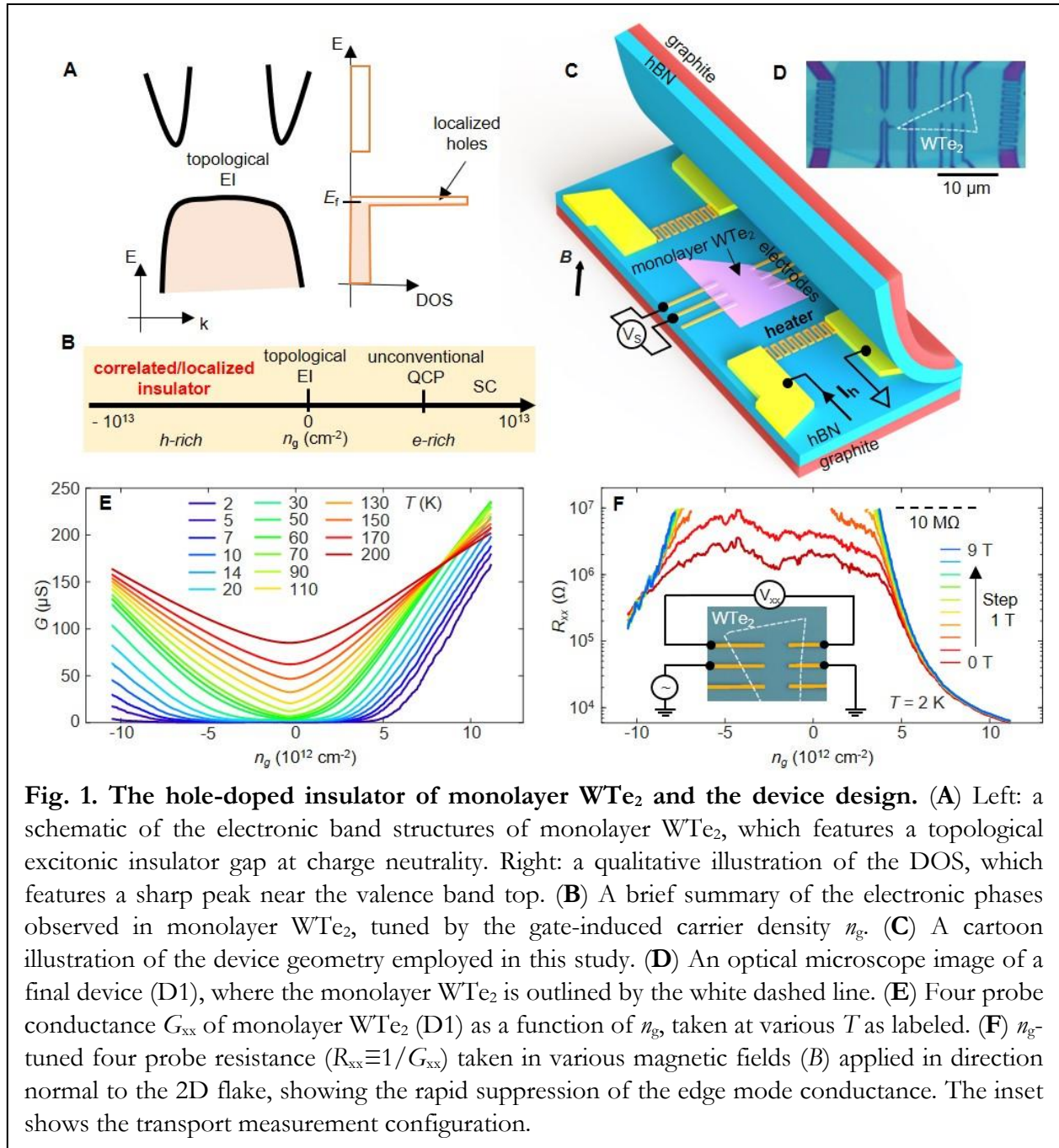
Authors declare that they have no competing interests.

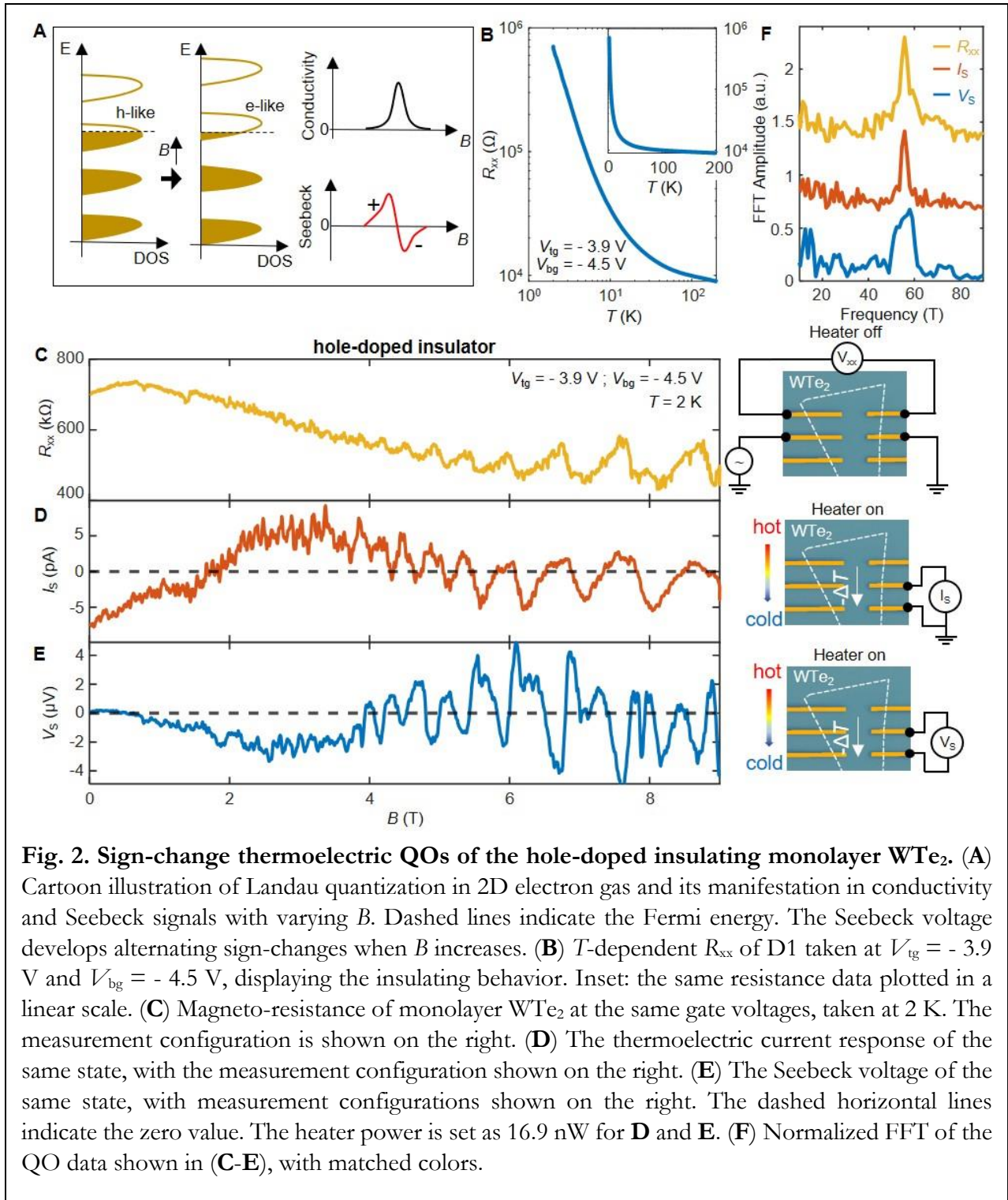
Data availability

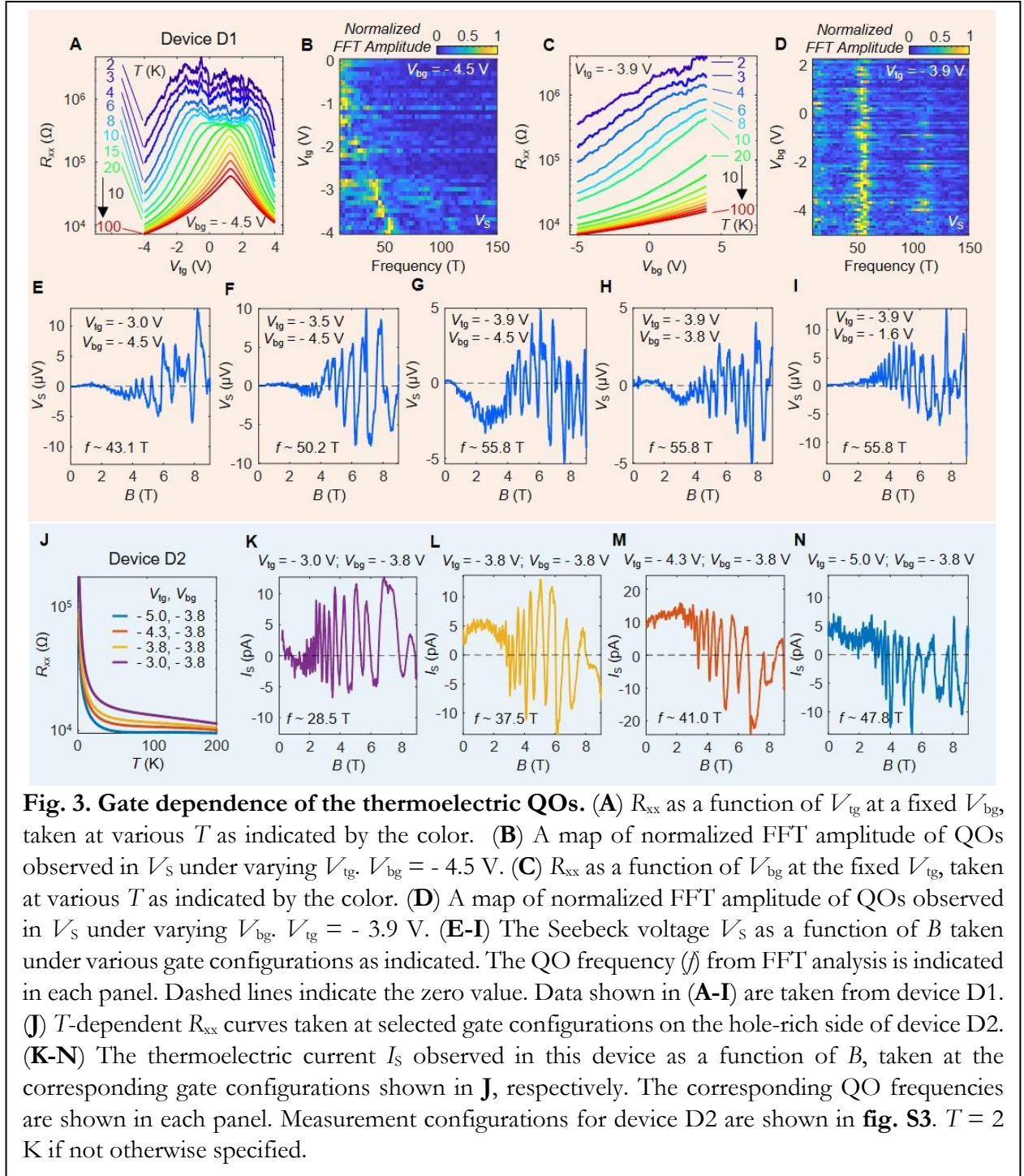
All data needed to evaluate the conclusions are presented in the paper. Additional data related to this paper are available from the corresponding author upon reasonable request.

Supplementary Materials:

Materials and Methods
Supplementary Text
Figs. S1 to S5
References







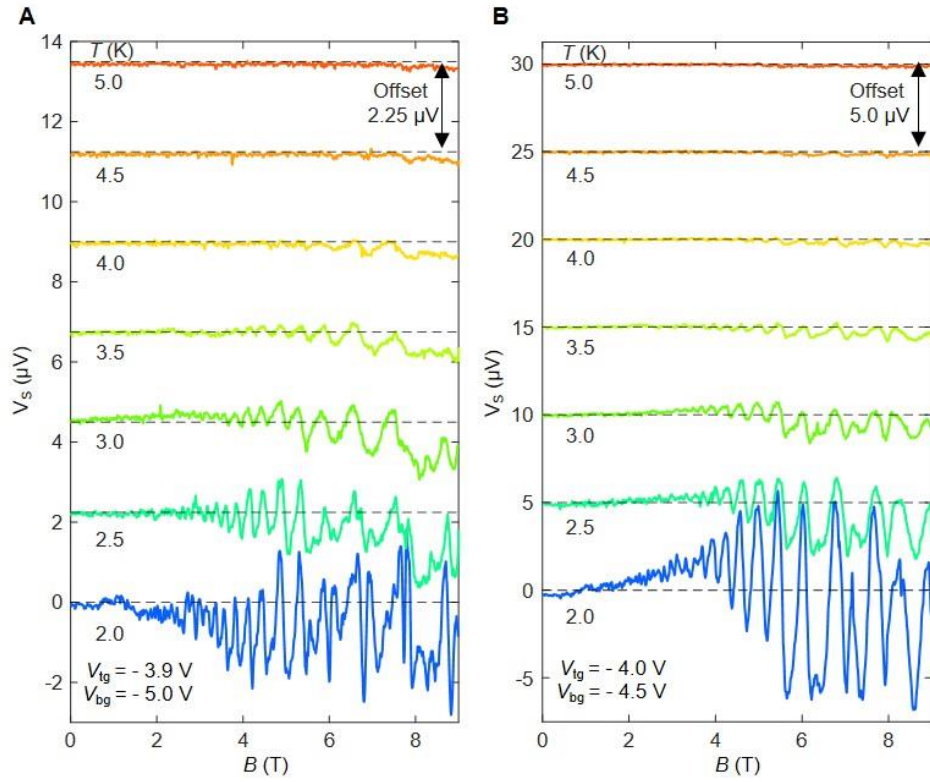


Fig. 4. Temperature dependence of the QOs. (A) V_s as a function of B , taken at $V_{\text{tg}} = -3.9$ V and $V_{\text{bg}} = -5.0$ V, at various T as indicated. **(B)** The same measurement but taken at $V_{\text{tg}} = -4.0$ V and $V_{\text{bg}} = -4.5$ V. Data are taken from device D1. The curves are offset by a constant in y axis for a better visualization and the zero value of V_s for each curve are indicated as the dashed line.

Supplementary Materials for

Sign-Alternating Thermoelectric Quantum Oscillations and Insulating Landau Levels in Monolayer WTe₂

Yue Tang¹, Tiancheng Song¹, Haosen Guan¹, Yanyu Jia¹, Guo Yu^{1,2}, Zhaoyi Joy Zheng^{1,2}, Ayelet J. Uzan¹, Michael Onyszczak¹, Ratnadwip Singha³, Xin Gui³, Kenji Watanabe⁴, Takashi Taniguchi⁵, Robert J. Cava³, Leslie M. Schoop³, N. P. Ong¹, Sanfeng Wu^{1*}

¹Department of Physics, Princeton University, Princeton, New Jersey 08544, USA.

²Department of Electrical and Computer Engineering, Princeton University, Princeton, New Jersey 08544, USA.

³Department of Chemistry, Princeton University, Princeton, New Jersey 08544, USA.

⁴Research Center for Electronic and Optical Materials, National Institute for Materials Science, 1-1 Namiki, Tsukuba 305-0044, Japan

⁵Research Center for Materials Nanoarchitectonics, National Institute for Materials Science, 1-1 Namiki, Tsukuba 305-0044, Japan

*Correspondence to: sanfengw@princeton.edu

This PDF file includes:

Materials and Methods

Figs. S1 to S5

References

Materials and Methods

Device fabrication

The procedure of device fabrication is similar to that described in our previous works(5, 9, 10). (i) We first fabricated a bottom van der Waals (vdW) stack consisting of hexagonal boron nitride (hBN) and graphite flakes, followed by depositing a thin layer of metal electrodes and the heaters on the stack. The hBN and graphite flakes were mechanically exfoliated onto 285 nm SiO₂/Si substrates and selected after the examinations under optical and atomic force microscopes (AFM). The standard 2D dry transfer technique was employed for creating the bottom graphite/hBN stack on a SiO₂/Si (insulating) substrate with prepatterned Ti/Au metal pads for wire bonding as well as alignment markers. The thin metal electrodes and microheaters (2 nm Ti/10 nm Pd) were deposited on top of the bottom vdW stacks, followed by another deposition of 5 nm Ti/55 nm Au that connects the thin electrodes on the vdW stack to the prepatterned thick metal wire-bond pads. All metals are patterned and deposited using the standard e-beam lithography and metal deposition tools in a clean room. (ii) the prepatterned bottom stack are then cleaned and examined carefully under AFM to confirm its cleanness with an atomic resolution. The AFM tip cleaning procedure using the contact mode is typically applied to make sure the best quality of the surface. (iii) Another key part of the device is a high-quality top stack consisting of graphite/hBN/monolayer WTe₂. High-quality WTe₂ bulk crystals were exfoliated onto 285 nm SiO₂/Si substrates in an argon-filled glovebox (with water and oxygen concentrations less than 0.1 ppm). Monolayer WTe₂ flakes were identified by the standard optical contrast that was routinely applied. The same dry transfer technique was employed to make the top hBN/graphite/WTe₂ stack, which was released onto the pre-patterned bottom stack in the glovebox. The optical and AFM images at selected stages of the process and more details about the device structures can be found in **fig. S1**.

Electrical transport measurements

The electrical transport measurement was conducted in a Quantum Design Dynacool system (with a base temperature of ~ 1.8 K), equipped with a superconducting magnet (up to 9 T). Four-probe resistance measurements were performed using the standard ac lock-in technique with a low frequency ~ 7 Hz. A small voltage excitation of 2 mV typically is applied to the source electrodes while the current flow through the drain is measured with a current preamplifier (DL Instrument 1211). The voltage drop between two longitudinal probes are recorded with a low noise voltage preamplifier (DL Instrument 1201).

Thermoelectric measurements

In the thermoelectric measurement, a current is applied to a microheater (of resistance ~ 10 K Ω) fabricated next to the monolayer WTe₂ to generate a temperature gradient. As illustrated in Fig. 1C, the microheater is made of a thin, narrow and curved metal stripe (~ 200 nm wide and ~ 12 nm thick). During measurements (configurations shown in Figs. 2D & E), an alternating current was applied to a microheater at low frequency of $\omega \sim 4$ Hz, which produces an alternating temperature gradient oscillating at the frequency of 2ω . The lock-in technique is employed to extract thermoelectric signals (V_s or I_s) at the frequency of 2ω , like the standard electrical transport measurements. The same device structure and measurement technique has been applied successfully to detect the vortex Nernst signals(9) of monolayer WTe₂. The effect of heater power is shown in **fig. S5**.

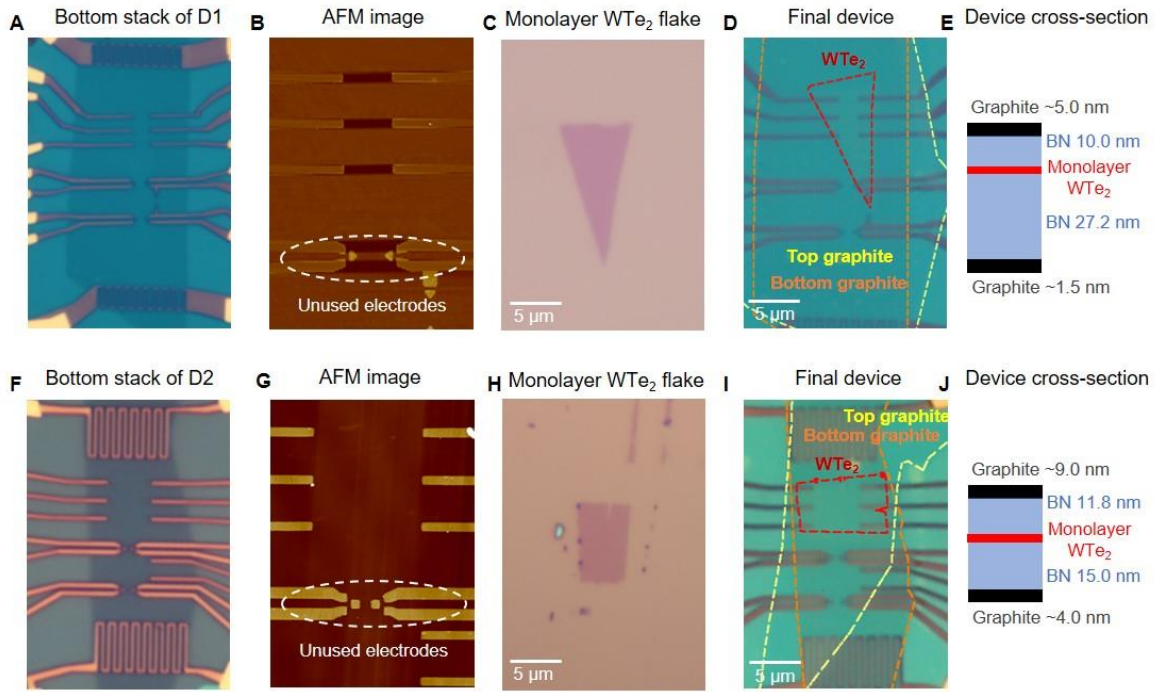


Fig. S1. Details of device fabrication. (A) Bottom graphite/hBN stack and metal electrodes of device D1. (B) an AFM image of the prepatterned bottom stack shown in A. (C) An optical microscope image of monolayer WTe_2 flake used for D1. (D) An optical microscope image of the final device D1. The red dashed line highlights the monolayer WTe_2 flake while yellow and orange dashed lines outline the top and bottom graphite layers, respectively. (E) Schematic of the cross section of device D1, with the thickness of each layers indicated. (F-J) The same description of device D2, with an optical image of the bottom stack (F), an AFM image (G), the monolayer WTe_2 flake (H), an optical image of the final device (I), and the cross-section schematic (J).

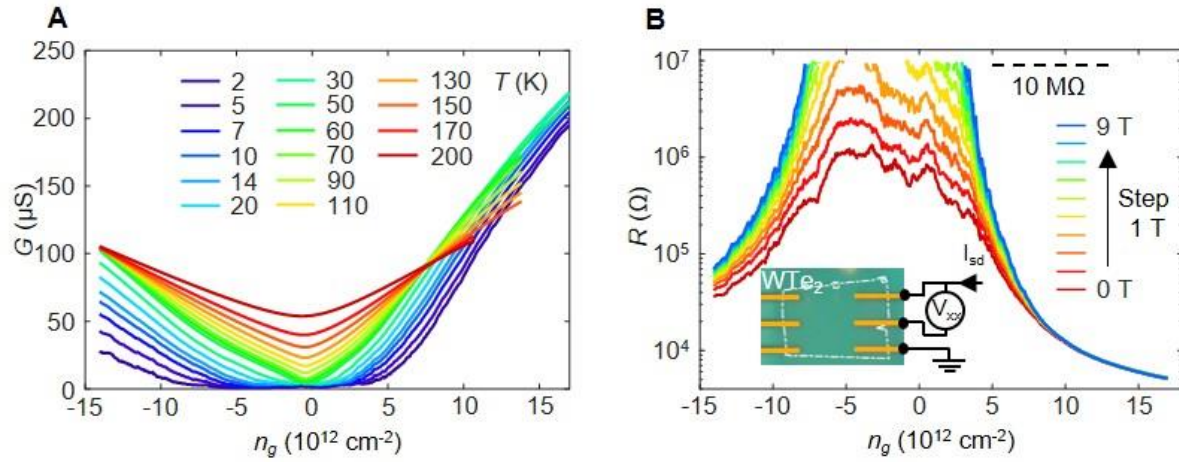


Fig. S2. Electrical transport characterization of device D2. (A) The conductance G of monolayer WTe_2 as a function of n_g taken at various T as labeled. (B) The resistance ($R \equiv 1/G$) tuned by n_g taken in various B. The measurement geometry is shown as an inset of B.

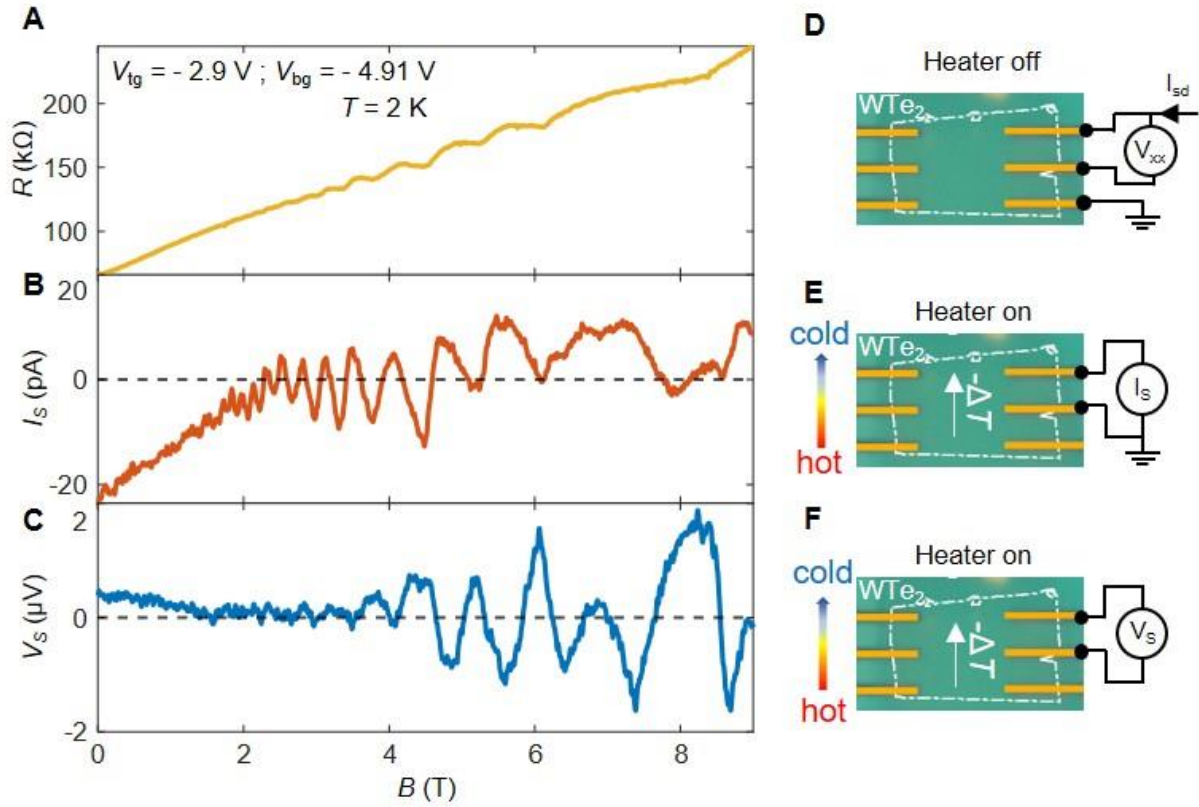


Fig. S3. Sign-change thermoelectric QOs of the hole-doped monolayer WTe_2 in device D2. (A) Magnetoresistance of monolayer WTe_2 of device D2 taken at $V_{\text{tg}} = -2.9$ V and $V_{\text{bg}} = -4.91$ V. The measurement configuration is shown on the right. (B) The thermoelectric current response of the same state, with the measurement configuration shown on the right. (C) The Seebeck voltage of the same state, with measurement configurations shown on the right. The dashed horizontal lines indicate the zero value.

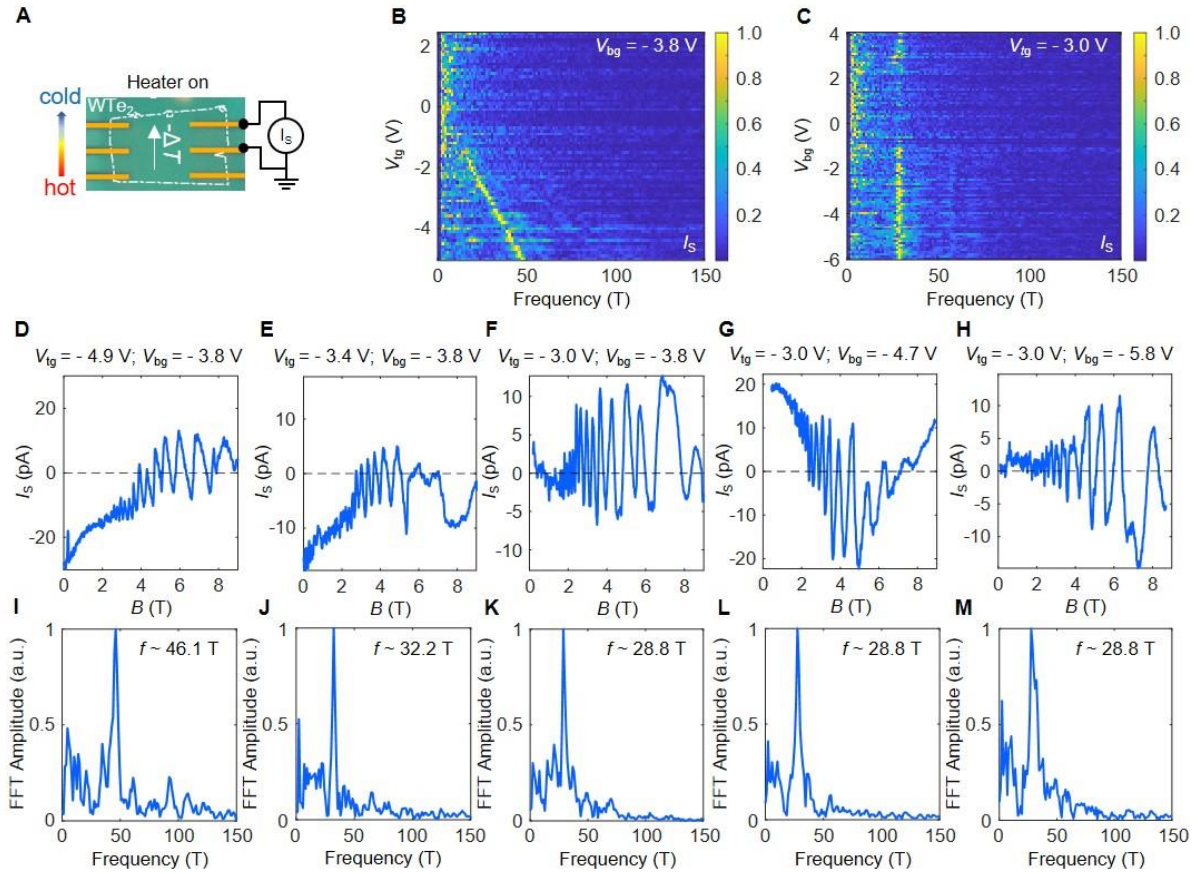


Fig. S4. Gate dependence of thermoelectric QOs in device D2. (A) Measurement configuration for detecting the thermoelectric current (I_s). (B) A map of normalized FFT amplitude of QOs observed in I_s under varying V_{tg} . $V_{bg} = -3.8$ V. (C) A map of normalized FFT amplitude of QOs observed in I_s under varying V_{tg} . $V_{bg} = -3.0$ V. (D-H) I_s as a function of B taken under various gate configurations as indicated. Dashed lines indicate the zero value. (I-M) Normalized FFT of the QO data shown in (D-H). The QO frequency (f) from FFT analysis is indicated in each panel.

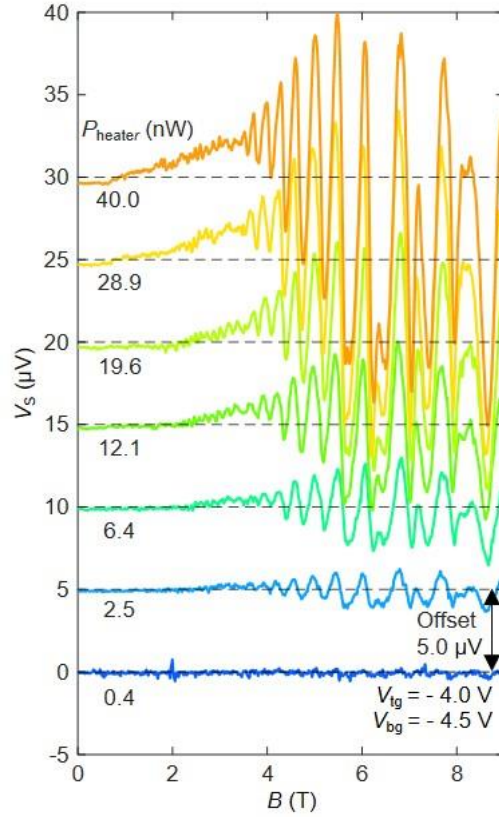


Fig. S5. Heater-power dependence of the QOs. V_S as a function of B , taken at $V_{tg} = -4.0$ V and $V_{bg} = -4.5$ V, under the application of different heater power (P_{heater}) as indicated. Data is taken in device D1. For clarity the curves are offset by $5 \mu\text{V}$ with respect to each other. The dashed lines indicate the zero value of V_S for each curve.